AGU PUBLICATIONS

Global Biogeochemical Cycles

RESEARCH ARTICLE
10.1002/2015GB005338

Key Points:
- The sources of uncertainty in global and regional projections are quantified
- Internal variability uncertainty is dominant on small spatial scales and short time horizons
- Model and scenario uncertainties become dominant in end-of-century projections

Supporting Information:
- Supporting Information S1

Correspondence to:
T. L. Frölicher,
thomas.froelicher@usys.ethz.ch

Citation:
Frölicher, T. L., K. B. Rodgers, C. A. Stock, and W. W. L. Cheung (2016), Sources of uncertainties in 21st century projections of potential ocean ecosystem stressors, *Global Biogeochem. Cycles*, *30*, 1224–1243, doi:10.1002/2015GB005338.

Received 24 NOV 2015
Accepted 12 AUG 2016
Accepted article online 15 AUG 2016
Published online 31 AUG 2016

Sources of uncertainties in 21st century projections of potential ocean ecosystem stressors

Thomas L. Frölicher[1], Keith B. Rodgers[2], Charles A. Stock[3], and William W. L. Cheung[4]

[1]Environmental Physics, Institute of Biogeochemistry and Pollutant Dynamics, ETH Zürich, Zürich, Switzerland, [2]Program in Atmospheric and Oceanic Sciences, Princeton University, Princeton, New Jersey, USA, [3]NOAA Geophysical Fluid Dynamics Laboratory, Princeton, New Jersey, USA, [4]NF-UBC Nereus Program and Changing Ocean Research Unit, Institute for the Oceans and Fisheries, University of British Columbia, Vancouver, British Columbia, Canada

Abstract Future projections of potential ocean ecosystem stressors, such as acidification, warming, deoxygenation, and changes in ocean productivity, are uncertain due to incomplete understanding of fundamental processes, internal climate variability, and divergent carbon emission scenarios. This complicates climate change impact assessments. We evaluate the relative importance of these uncertainty sources in projections of potential stressors as a function of projection lead time and spatial scale. Internally generated climate variability is the dominant source of uncertainty in middle-to-low latitudes and in most coastal large marine ecosystems over the next few decades, suggesting irreducible uncertainty inherent in these short projections. Uncertainty in projections of century-scale global sea surface temperature (SST), global thermocline oxygen, and regional surface pH is dominated by scenario uncertainty, highlighting the critical importance of policy decisions on carbon emissions. In contrast, uncertainty in century-scale projections of net primary productivity, low-oxygen waters, and Southern Ocean SST is dominated by model uncertainty, underscoring that the importance of overcoming deficiencies in scientific understanding and improved process representation in Earth system models are critical for making more robust projections these potential stressors. We also show that changes in the combined potential stressors emerge from the noise in 39% (34–44%) of the ocean by 2016–2035 relative to the 1986–2005 reference period and in 54% (50–60%) of the ocean by 2076–2095 following a high-carbon emission scenario. Projected large changes in surface pH and SST can be reduced substantially and rapidly with aggressive carbon emission mitigation but only marginally for oxygen. The regional importance of model uncertainty and internal variability underscores the need for expanded and improved multimodel and large initial condition ensemble projections with Earth system models for evaluating regional marine resource impacts.

1. Introduction

Ocean ecosystems are increasingly stressed by human-induced climate change affecting their physical and biogeochemical environment [*Halpern et al.*, 2008; *Crain et al.*, 2008; *Hoegh-Guldberg and Bruno*, 2010; *Doney et al.*, 2012; *Pörtner et al.*, 2014]. Warming, acidification, deoxygenation, and changes in primary productivity by marine phytoplankton have been identified as key potential ocean ecosystem stressors that may challenge sustainable management of living marine resources under climate change [*Gruber*, 2011; *Doney et al.*, 2012; *Hall et al.*, 2013; *Pörtner et al.*, 2014; *Gattuso et al.*, 2015].

On a global scale, the evolution of these drivers is largely a consequence of rising atmospheric CO_2 levels and associated climate change. The ocean has taken up approximately 28% of anthropogenic carbon emissions since preindustrial levels [*Sabine et al.*, 2004; *Frölicher et al.*, 2015], slowing the increase in atmospheric CO_2. However, the uptake of anthropogenic CO_2 drives ocean acidification, specifically a decrease in both pH and the saturation state of seawater with regard to mineral calcium carbonate, both being critical drivers of solubility of shells and skeletons for many marine organisms [*Doney et al.*, 2009]. Ocean acidification may also affect other biological processes such as reproduction, growth, feeding, and behavior [*Kroeker et al.*, 2013]. In addition, the ocean has absorbed nearly 93% of the Earth's excess heat since the 1970s, which has offset a large part of atmospheric warming but also causes warmer oceans [*Rhein et al.*, 2013]. The warming and in many regions freshening of the ocean tends to stratify the upper ocean [*Manabe et al.*, 1991; *Sarmiento et al.*, 1998; *Capotondi et al.*, 2012], leading not only to a reduced supply of nutrients to the surface ocean and decreasing net primary productivity (NPP) [*Bopp et al.*, 2001; *Steinacher et al.*, 2010] but also to a reduced resupply of oxygen to the ocean's interior sustaining deoxygenation and an expansion of low-oxygen waters

[*Frölicher et al*., 2009; *Keeling et al*., 2010]. In the coming decades, rising atmospheric CO_2 levels may amplify the magnitude of changes in these potential ocean ecosystem stressors. These changes in ocean properties likely affect the marine biogeochemical cycles, species biogeography and phenology, ecosystem dynamics, and ultimately the ecosystem services to human society [*Pörtner et al*., 2014; *Gattuso et al*., 2015].

While theoretical arguments and Earth system models (ESMs) project a warmer and more acidified global ocean under increasing atmospheric CO_2 levels, there are significant disagreements in projected trends [*Bopp et al*., 2013]. These disagreements can be stark for global and regional NPP [*Steinacher et al*., 2010; *Bopp et al*., 2013; *Laufkötter et al*., 2015] and regional subsurface O_2 concentrations [*Cocco et al*., 2013]. For example, one ESM projects a decrease in global NPP of about 7 Pg C/yr over the 21st century, whereas another projects almost no change under the same high business-as-usual future emission scenario (Figure 1j [*Bopp et al*., 2013]). At regional scales, even the direction of projected changes of low O_2 waters (Figures 1h and 1i [*Cocco et al*., 2013]) and NPP (Figures 1k and 1l [*Steinacher et al*., 2010]) varies from model to model. This reflects significant gaps in our understanding of the physical and biological processes dictating and regulating changes in the potential ocean ecosystem stressors.

At present, the marine biogeochemical community trails behind their physical oceanographic counterparts in terms of skill and uncertainty assessment of their future projections. This is of particular concern as ocean ecosystems provide a wide range of services to human society. It also currently limits the use of ESMs to force global and regional impact models through downscaling [*Cheung et al*., 2013, 2016]. Statements of confidence concerning the impact of climate change on living marine resources within the Intergovernmental Panel on Climate Change Fifth Assessment Report Working Group II report were based on a qualitative assessment of observational evidence and individually published projections [*Pörtner et al*., 2014]. While this is a necessary starting point, improved understanding of projection uncertainty at temporal and spatial scales that are relevant to management decision making, including stock recovery plans and industry capitalization, is crucial and requires accurate uncertainty assessments, especially in very productive ocean regions [*Link et al*., 2012].

The uncertainty in projections of potential ocean ecosystem stressors may arise from three fundamentally distinct sources [*Hawkins and Sutton*, 2009, 2011]. First, *internal variability uncertainty* stems from natural variability inherent in the coupled carbon-climate system in the absence of any radiative perturbations [*Lorenz*, 1963; *Frölicher et al*., 2009; *Deser et al*., 2012, 2014]. Internally generated climate variability reflects phenomena such as the El Niño–Southern Oscillation (ENSO) [*Cane and Zebiak*, 1985] or the Atlantic Multidecadal Oscillation and has the potential to alter—sometimes over several decades—the longer-term trends that are associated with anthropogenic changes. Internal variability also includes natural variability on smaller scales unrelated to climate modes. The second source of uncertainty is the *model uncertainty*. Different models may yield different responses to the same radiative forcing. An important source of this uncertainty lies in the implementation of different physical and biogeochemical modules in the individual models and their underlying parameterizations. The third source of uncertainty, termed *scenario uncertainty*, arises from present and future policy decisions impacting greenhouse gas emissions, as well as technological and sociological factors that are not yet determined. Scenario uncertainty differs from internal variability uncertainty and model uncertainty as it quantifies divergence between alternative policy prescriptions rather than inherent model prediction uncertainties. The full range of possible future changes in potential ocean ecosystem stressors reflects contributions from all of these three uncertainty sources, with potential cases of uncertainty interacting and accumulating over components of the Earth system.

Systematic exploration of contributions of these uncertainty sources across spatial scales and time horizons has been previously evaluated for surface air temperature and precipitation [e.g., *Hawkins and Sutton*, 2009, 2011; *Yip et al*., 2011; *Booth et al*., 2013], for steric sea level changes [*Little et al*., 2015; *Bordbar et al*., 2015], and for air-sea CO_2 fluxes [*Lovenduski et al*., 2016]. However, systematic analyses across all three uncertainty sources are lacking for projections of potential ocean ecosystem stressors. Previous work has assessed contributions of scenario and model uncertainty to potential ocean ecosystem stressor projections across the relatively small ESM ensemble but has omitted assessment of irreducible uncertainty associated with internal climate variability [*Bopp et al*., 2013]. Different methods such as preindustrial control simulations, detrended transient forced simulations, and large "perturbed initial condition" ensembles [e.g., *Frölicher et al*., 2009] are usually used to assess this component of projection uncertainty, which has been found to be particularly

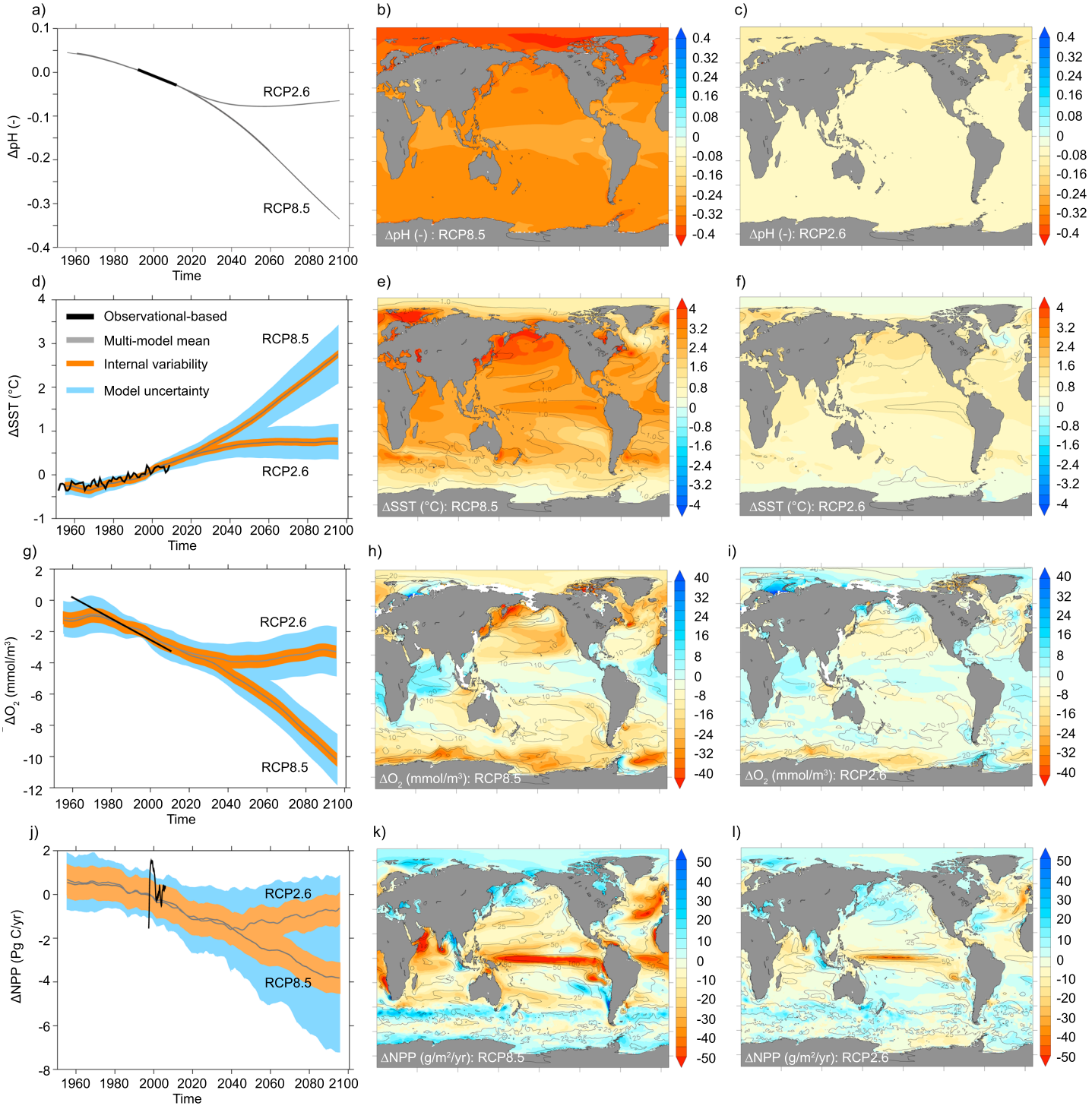

Figure 1. Time series and spatial patterns of simulated change in surface pH, sea surface temperature, O_2 concentration averaged over 100 to 600 m depth, and NPP integrated over the top 100 m. (left column) Observation-based estimates (black lines) and simulated global changes over the period of 1950 to 2100. Simulated spatial patterns of multimodel mean changes in year 2085 (2076–2095 average) for the (middle column) RCP8.5 scenario and (right column) RCP2.6 scenario. All changes are shown relative to the 1985–2004 period. In the left column, the gray lines indicate the CMIP5 multimodel mean for the two scenarios RCP2.6 and RCP8.5 and uncertainty range indicates internal variability (orange) and model uncertainty (blue). In the middle and right columns, the contours indicate the sum of model uncertainty and internal variability uncertainty. Observation-based estimates for surface pH are from *Lauvset et al.* [2015], for SST from *Smith et al.* [2008], for O_2 at 300 dbar from *Stramma et al.* [2012], and for NPP from *Behrenfeld et al.* [2006]. Only trends are given for surface pH and O_2 observations. Reference periods for observed pH, O_2, and NPP changes are arbitrarily chosen.

prominent at local to regional scales and over early to middle century time horizons for surface temperature and precipitation [*Hawkins and Sutton*, 2009, 2011; *Deser et al*., 2012], high-latitude sea surface temperature (SST), low-latitude O_2 concentrations [*Frölicher et al*., 2009], and global NPP [*Rodgers et al*., 2015]. However, it remains unclear which source of uncertainty is dominant in projections of potential ecosystem stressors on different spatial scales and time horizons and how the uncertainty sources vary across the four different potential stressors.

This study aims to quantify the evolution of these three sources of projection uncertainty in potential ocean ecosystem stressors over this century by using output from a range of ESMs contributed to Coupled Model Intercomparison Project phase 5 (CMIP5). The remainder of the study is structured as follows: the model simulations and the calculation of uncertainty and time of emergence are introduced in section 2. Section 3 presents the sources of uncertainty on different spatial scales and time horizons as well as the time of emergence of signals in changes of potential ocean ecosystem stressors from underlying uncertainty. We also discuss the sensitivity of the results to various options for estimating internal variability, including the use of a large initial condition ensemble from one Earth system model. A discussion and conclusion follow in section 4.

2. Methods

2.1. CMIP5 Model Simulations

To assess internal variability and model and scenario uncertainties, we make use of Earth system models that participated in the Coupled Model Intercomparison Project phase 5 (CMIP5) [*Taylor et al*., 2012] and that were run over the 1950–2100 period under historical and the Representative Concentration Pathway (RCP)8.5 and the RCP2.6 scenarios [*Van Vuuren et al*., 2011]. RCP8.5 is a high-carbon emission, business-as-usual scenario with a net radiative forcing by year 2100 of 8.5 W/m^2 and a simulated global atmospheric surface temperature change of about 3.7 ± 0.7°C relative to 1986–2005 [*Collins et al*., 2013]. RCP2.6 is a stringent emission mitigation scenario with a global mean net radiative forcing by year 2100 of 2.6 W/m^2 and a simulated global atmospheric surface temperature change of about 1.0 ± 0.4°C [*Collins et al*., 2013]. We also make use of century-long (≥252 years) preindustrial control simulations.

We analyze 20 different CMIP5 Earth system models, but only a subset of these includes ocean biogeochemistry (Table S1 in the supporting information). Note that not all scenarios and preindustrial control simulations were available for all models. All CMIP5 model fields have been regridded onto a regular 1° × 1° grid. The skill of a subset of models in representing observed distributions in the four potential ocean ecosystem stressors has been evaluated elsewhere [e.g., *Bopp et al*., 2013].

2.2. Separating the Sources of Uncertainty

Although there is no perfect way to clearly separate the different uncertainties, different methods have given similar results [*Hawkins and Sutton*, 2009; *Yip et al*., 2011; *Lyu et al*., 2015]. Here the *total uncertainty* (*T*) is the sum of the *scenario uncertainty* (*S*) driven by the forcing scenarios RCP2.6 and RCP8.5, the *model uncertainty* (*M*) obtained from the different CMIP5 ESM projections, and the *internal variability uncertainty* (*I*) obtained from century-long preindustrial control simulations of the CMIP5 ESMs:

$$T(x,y,t) = S(x,y,t) + M(x,y,t) + I(x,y,t). \quad (1)$$

The *scenario uncertainty* (*S*) is calculated as the difference between the multimodel mean projections of the CMIP5 ESMs following the RCP8.5 scenario $\left(\overline{\mathrm{CMIP5}_{\mathrm{RCP8.5}}}\right)$ and the multimodel mean projections of the CMIP5 models following the RCP2.6 scenario $\left(\overline{\mathrm{CMIP5}_{\mathrm{RCP2.6}}}\right)$:

$$S(x,y,t) = \overline{\mathrm{CMIP5}_{\mathrm{RCP8.5}}(x,y,t)} - \overline{\mathrm{CMIP5}_{\mathrm{RCP2.6}}(x,y,t)}. \quad (2)$$

Note that the RCP scenarios may not sample the full range of uncertainty in future anthropogenic forcing. For example, anthropogenic aerosols are assumed to decline quite rapidly in both RCP scenarios in the next 20 years. We also do not consider any nonlinear dependence of the climate model response on the scenario (i.e., models react differently to emission scenarios) [*Yip et al*., 2011]. Averaging over the multimodel ensemble in equation (2) suppresses variations due to internal variability. However, the multimodel ensemble is small, so we take the further step of filtering with a 10 year running mean (i.e., longer than the typical

ENSO period) before calculating the multimodel means to further minimize the potential for internal variability uncertainty to contaminate scenario uncertainty estimates. The sensitivity to 10 year low-pass filtering is analyzed in section 4.

The *model uncertainty* (*M*) is calculated as the mean of the 1 standard deviation (SD) between the individual CMIP5 RCP8.5 model projections SD($CMIP5_{RCP8.5}$) and the 1 standard deviation between the individual CMIP5 RCP2.6 model projections SD($CMIP5_{RCP2.6}$):

$$M(x,y,t) = \frac{\mathrm{SD}(\mathrm{CMIP5}_{\mathrm{RCP8.5}}(x,y,t)) + \mathrm{SD}(\mathrm{CMIP5}_{\mathrm{RCP2.6}}(x,y,t))}{2}. \quad (3)$$

As with the scenario uncertainty, we filter simulated changes with a 10 year running mean before calculating standard deviations to minimize the potential for contamination of *M*(*x*,*y*,*t*) with internal variability uncertainty. The CMIP5 ensemble is an ensemble of opportunity, and the CMIP5 models should likely not be considered as independent models [*Knutti et al*., 2013]. *Murphy et al.* [2004], for example, suggest that uncertainty with atmospheric temperature projections coming from unknown parameters in the Hadley Centre Coupled Model version 3 is about equal to that in the CMIP ensembles. For the biogeochemical system with more underconstrained parameters than in the physical models, we expect that our method potentially undersamples the overall model uncertainty.

The internal variability uncertainty (*I*) is calculated as the multimodel mean of 1 standard deviation of linearly detrended century-long preindustrial control simulations of the CMIP5 ESMs ($\overline{\mathrm{CMIP5}_{\mathrm{Ctrl}}}$)

$$I(x,y,t) = \overline{\mathrm{SD}(\mathrm{CMIP5}_{\mathrm{Ctrl}}(x,y,t))} \quad (4)$$

We make the assumption that internal variability does not change with time and is unaffected by greenhouse gas forcing [*Hawkins and Sutton*, 2009]. Sensitivity of our results to this assumption is discussed in sections 2.4 and 3.5. The coarse resolution CMIP5 ESMs do not capture potentially large internal variability associated with submesoscale and mesoscale ocean features such as fronts, eddies, and filaments [*Rodgers et al*., 2009; *Stock et al*., 2011]. Thus, internal variability uncertainty may be larger than estimated herein on small spatial scales.

For all analysis in this study, we use annual mean fields. This means that reported absolute and partitioned uncertainties reflect the estimated contributions of each source to annual conditions, either for a given year (when plotted as a time series) or value characteristic of a set of years where specified. From a marine resource perspective, this addresses the question if the state of a potential ocean ecosystem stressor for a given year will be primarily dictated by the state of climate variability, by the emission scenario we choose, or by the model response that is closest to the truth.

We note that there is an implicit assumption in our methodology that model and scenario uncertainty will be manifested through divergences across decadal scales. Pragmatically, filtering *M*(*x*,*y*,*t*) and S(*x*,*y*,*t*) with a 10 year running mean prior to calculation was an accommodation dictated by the small multimodel ensemble size. Averaging over six model members used for oxygen and seven model members used for pH for the RCP2.6 scenario, for example (Table S1), cannot fully suppress contributions from internal variability. It is consistent, however, with the regular globally coherent divergence of greenhouse gas (GHG) concentrations over decadal scales and the presumption that model response uncertainty to such GHG accumulation is similar in character. Details of the solutions are somewhat sensitive to these choices—not filtering *M*(*x*,*y*,*t*) and *S*(*x*,*y*,*t*) with a 10 year running mean boosts their importance. Sensitivity to these choices will be discussed in section 4 but does not fundamentally change the emergent trends in importance highlighted in section 3.

2.3. Calculation of Signal-to-Noise Ratios and Time of Emergence

The signal-to-noise (S/N) ratio is calculated for both future emission scenarios using the ratio between the signal, defined as changes in the potential ocean ecosystem stressors relative to the 1986–2005 period ($\Delta_{\mathrm{stressors}}$), and the noise, defined as the model uncertainty plus the internal variability uncertainty ($M + I$):

$$\frac{S}{N} = \frac{\Delta_{\mathrm{stressors}}}{M + I} \quad (5)$$

Time of emergence is defined as the year at which the signal first reaches a value larger than the uncertainty due to internal and model uncertainties. We focus our analysis on a threshold of 1 for S/N representing a

confidence internal of 67% for significance as well as on a 20 year reference period to smooth out any remaining natural interannual to decadal variability. The choice of the reference period is somewhat arbitrary, but it facilitates comparison with earlier studies using the same reference period but focusing on the time of emergence of climate signals [e.g., *Hawkins and Sutton*, 2012; *Lyu et al*., 2014]. The definition of noise includes both internal variability uncertainty and model uncertainty, not comparable with the study of *Rodgers et al.* [2015], where they define the noise for the same variables as internal variability uncertainty only. Additionally, it is important to point out that *Rodgers et al.* [2015] used 30 year trends to define both the signal and noise components of signal to noise, and they analyzed time of emergence of signals relative to year 1965.

2.4. Sensitivity to Estimation of Internal Variability

The estimation of internal variability is a critical element of our analysis, and multiple approaches have been used in past studies. In our analysis, we use estimates from the preindustrial control simulations from multiple CMIP5 ESMs, because (i) existing ESMs exhibit substantial diversity with respect to the magnitude (and frequency) of internal variability [*Keller et al*., 2014; *Resplandy et al*., 2015], (ii) the usage of preindustrial control simulations provides a longer sample of years to characterize variability than using relatively short transient simulations, and (ii) extracting the variability signal from preindustrial simulations does not require subjective decisions about how to filter the climate change signal [*Hawkins and Sutton*, 2009; *Lovenduski et al*., 2016]. A disadvantage, however, is that the relatively small size of the multimodel ensemble may not fully capture low-frequency modes of variability [e.g., *Deser et al*., 2014], and preindustrial simulations do not allow for modes of variability to evolve under the forced climate change signal. Recent studies suggest that the implicit assumption that internal variability does not change under external forcing is inaccurate, for example, for the case of surface air temperature in northern high latitudes [*Huttingford et al*., 2013; *Screen*, 2014] but also for surface pH [*McNeil and Sasse*, 2016] and possibly for other variables of the nonlinear marine ecosystem and carbon chemistry system. We thus considered in section 3.5 two alternatives used elsewhere in the literature to test the robustness of our results to these assumptions.

The first alternative was to use the large 30-member ensemble simulation [*Rodgers et al*., 2015] of the coupled carbon-climate Earth system model (ESM2M) developed at the Geophysical Fluid Dynamics Laboratory (GFDL) [*Dunne et al*., 2012, 2013]. The ensemble of climate simulations was run under identical historical and RCP8.5 forcing over the period of 1950 to 2100, but each simulation was initialized with slightly different but equally plausible atmosphere-ocean-land-sea ice initial conditions [*Rodgers et al*., 2015]. While ensemble member 1 is a direct continuation of a simulation covering the period of 1861–1949, the ensemble members 2–30 use the state of ensemble member 1 at midnight of 1–29 January 1950 as their initial state on 1 January 1950. By considering each of the trajectories as a plausible outcome, the ensemble suite is used to deconvolve the forced (anthropogenic) response from the response associated with internal variability. It is the deviations of the individual ensemble members from the ensemble mean (the forced response) that facilitate a quantification of internal variability uncertainty. In fact, we calculate internal variability as the standard deviation of the 30-member ensemble simulations following the RCP8.5 scenario conducted with GFDL ESM2M. After calculating the standard deviation, a 10 year running mean filter has been applied, as $I(x,y,t)$ still exhibits interannual variability. The results, however, are not very sensitive to the length of this filter (not shown).

The second alternative was to use the multimodel CMIP5 transient simulation after filtering with a fourth-order polynomial as a proxy for the climate change signal. To avoid natural variations not associated with internal variability, we focus on the 2006–2100 period of the transient simulations as these simulations do not include variations in volcanic and solar forcing after 2006.

3. Results

3.1. Variability of Potential Ocean Ecosystem Stressor Projections

We first briefly discuss projections of the multimodel mean and total absolute variability in all four potential ocean ecosystem stressors (Figure 1) to provide necessary background for the uncertainty analysis. Detailed discussion of processes leading to the distinct global and regional changes can be found elsewhere [e.g., *Frölicher et al*., 2009; *Steinacher et al*., 2010; *Capotondi et al*., 2012; *Cocco et al*., 2013; *Bopp et al*., 2013; *Laufkötter et al*., 2015].

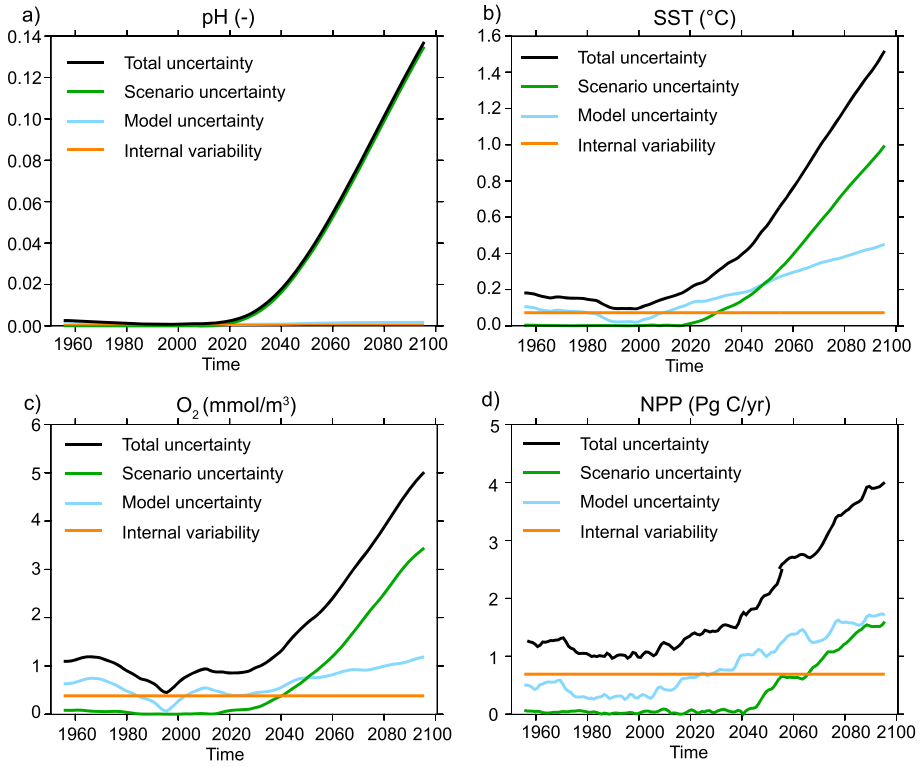

Figure 2. Times series of the total uncertainty, internal variability uncertainty, model uncertainty, and scenario uncertainty in projections of global annual mean changes in (a) surface pH, (b) SST, (c) O_2 averaged over 100–600 m, and (d) NPP integrated over top 100 m.

All models project ocean warming, acidification, deoxygenation, and changes in global NPP (Figure 1) [*Bopp et al.*, 2013; *Gattuso et al.*, 2015]. Simulated global changes over the last few decades are broadly consistent with observation-based estimates (black lines in Figures 1a, 1d, 1g, and 1j). By the end of the 21st century (2076–2095 relative to 1986–2005), pH is projected to decrease by 0.29 ± 0.00 (RCP8.5) and 0.07 ± 0.00 (RCP2.6; Figure 1a), SST is projected to increase by 2.39 ± 0.50°C (RCP8.5) and 0.75 ± 0.30°C (RCP2.6; Figure 1c), O_2 concentrations averaged over 100–600 m depth are projected to decrease by 6.98 ± 1.02 mmol/m^3 (RCP8.5) and 1.29 ± 1.06 mmol/m^3 (RCP2.6; Figure 1g), and depth-integrated NPP is projected to decrease by 3.58 ± 2.37 Pg C/yr (RCP8.5) and 0.85 ± 0.88 Pg C/yr (RCP2.6; Figure 1j).

The four potential ocean ecosystem stressors show distinct spatial patterns of changes for both the RCP8.5 and the RCP2.6 scenarios (Figure 1) [*Bopp et al.*, 2013; *Rodgers et al.*, 2015]. The pattern of projected multimodel mean surface pH change is spatially homogenous, with slightly larger reductions in the Arctic Ocean and smaller reductions in the low latitudes (Figures 1b and 1c). Largest warming of sea surface waters is projected to occur in the middle-to-high latitudes, whereas smallest warming is projected in the winter sea ice covered regions of the Arctic Ocean and in regions where deep convection occurs such as in the northern North Atlantic Ocean and the Southern Ocean (Figures 1e and 1f). Dissolved oxygen between 100 and 600 m is projected to decrease in the high latitudes due to reduced solubility of O_2 in warmer waters and reduced exchange between subsurface water and the atmosphere due to enhanced upper ocean density stratification (Figures 1h and 1i). However, O_2 is projected to increase in the low-oxygen regions of the low latitudes. In contrast to O_2, NPP is projected to decrease in most low-latitude regions due to stronger nutrient limitation as a result of increased stratification and/or temperature-driven increases in grazing and other loss processes (Figures 1k and 1l [*Laufkötter et al.*, 2015]). In the high latitudes, NPP is projected to increase due to warming and changes in light limitation [*Steinacher et al.*, 2010].

Large absolute model uncertainty plus internal variability uncertainty, as indicated with contour lines in spatial maps of Figure 1, is usually associated with regions that exhibit larger changes for both the RCP8.5 and RCP2.6 scenarios. There are exceptions, however. The North Atlantic exhibits large absolute uncertainty

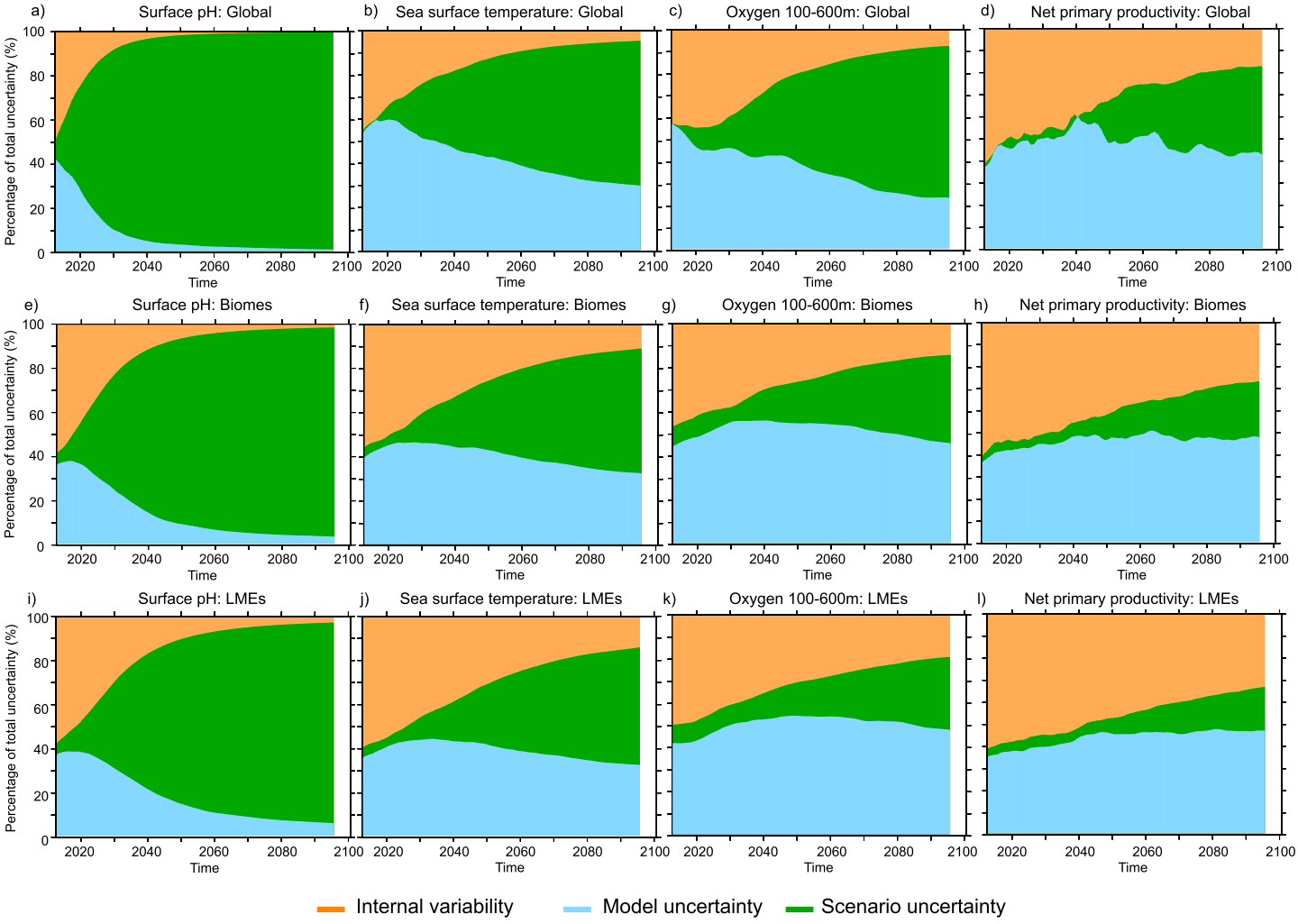

Figure 3. Fraction of total uncertainty explained by internal variability uncertainty (orange), model uncertainty (blue), and scenario uncertainty (green) in projections of annual mean surface pH, SST, O_2 averaged over 100 to 600 m, and NPP integrated over the top 100 m for (a–d) global projections, (e–h) projections averaged over 17 biogeographical biomes, and (i–l) projections averaged over 66 coastal large marine ecosystem (LME) areas.

in SSTs, whereas the projected multimodel mean change is relatively small (Figures 1e and 1f). In addition, the absolute uncertainty is larger than the magnitude of change for thermocline oxygen in the low-oxygen regions of the low latitudes (Figures 1h and 1i) [*Cocco et al.*, 2013] and almost everywhere for NPP (Figures 1k and 1l) [*Laufkötter et al.*, 2015] under both RCP scenarios.

3.2. Sources of Uncertainties on Global Scale

We decompose the temporal evolution of the uncertainty in global annual mean potential ocean ecosystem stressor projections into internal variability uncertainty, model uncertainty, and scenario uncertainty (Figures 2 and 3). In Figures 2 and 3, the mean changes for each individual model simulation are computed relative to 1986–2005. The total uncertainty (black lines in Figure 2) increases in time for all potential ocean ecosystem stressors. Whereas internal variability uncertainty remains constant (by definition) over the entire time period (orange lines in Figure 2), model uncertainty (blue line in Figure 2) and especially scenario uncertainty (green lines in Figure 2) largely increase over time. For an early and mid-21st century time horizon, the dominant sources of uncertainty are model and internal variability uncertainties. By the end of the century, scenario uncertainty dominates the total uncertainty for all four potential stressors, except for NPP, for which model uncertainty is larger than scenario and internal variability uncertainties.

The relative importance of the sources of uncertainty in global annual mean potential ocean ecosystem stressor projections as a function of projection time horizon is shown in Figures 3a–3d. Internal variability

uncertainty (orange area in Figures 3a–3d) is large over the near term for all variables and becomes relatively unimportant by the end of the 21st century. For surface pH, scenario uncertainty becomes dominant (explaining more than 50% of total uncertainty) after year 2021 and accounts for more than 98% of the uncertainty in global surface pH projections by the end of the century (Figure 3a). This largely reflects the tight coupling between surface ocean pCO_2 and atmospheric pCO_2, as atmospheric pCO_2 increases to 850 ppm in RCP8.5 by the end of the century but only to 426 ppm in RCP2.6. For SST, scenario uncertainty becomes dominant after year 2058, but the diminishment of both model uncertainty (30% of total uncertainty by the end of 21st century) and internal variability uncertainty (5%) progresses much more slowly than for surface pH (Figure 3b). For oxygen, the evolution of the sources of uncertainties is similar as for SST, except that internal variability uncertainty remains relatively high through the near term (44% in year 2025), with the proportion of total uncertainty due to the model uncertainty decreasing. For NPP, model uncertainty is responsible for more than half of the uncertainty through nearly the entire 21st century, diminishing to 43% only near the end of the 21st century.

The starkest contrast in Figures 3a–3d is between the dominance of the scenario uncertainty for global surface pH and the dominance of the model uncertainty and internal variability uncertainty for global NPP, with both SST and O_2 concentrations falling between the surface pH and NPP responses. The reduction in the importance of internal variability uncertainty over time reflects the increased prominence of scenario uncertainty and continued prominence of intermodel spread.

3.3. Sources of Uncertainties on the Biome, Large Marine Ecosystem, and Local Scale

Next, the uncertainty in potential ocean ecosystem stressor projections is partitioned on regional to local scale. We focus our analysis first on 17 biogeographical biomes (Figure S1 in the supporting information), before we discuss the sources of uncertainties in coastal large marine ecosystems (LMEs; Figure S2) and locally in the entire global open ocean. The 17 biogeographical biomes capture patterns of large-scale biogeochemical function at the basin scales and are defined by distinct SSTs, maximum mixed layer depths, maximum ice fractions, and summer chlorophyll concentrations [*Fay and McKinley*, 2014]. Large marine ecosystems host more than three quarters of world's annual marine fishery yields [*Pauly et al*., 2008] and have been adopted as discrete integrated regions over which to implement ecosystem-based marine resource management. They are characterized by similarities in bathymetry, hydrography, biological production, and trophic relationships [*Sherman and Alexander*, 1986]. Detailed analysis of uncertainty for each individual biome and LME can be found in Figures S3–S18.

Analysis of sources of uncertainty in annual mean potential ocean stressor states across biomes (Figures 3e–3h) and LMEs (Figures 3i–3l) show pronounced variations in the progression of uncertainty sources on different time horizons. For near-term time horizons (2016–2035), the contribution of internal variability uncertainty to annual conditions averaged over all LMEs and stressors (46%; orange area) is generally more prominent than for averages over all biomes (41%) and for global averages (32%). Internal variability uncertainty is the dominant uncertainty for SST, NPP, and even surface pH in projections over the next few decades averaged over all biomes (Figures 3e–3h) and LMEs (Figures 3i–3l). For example, in the equatorial Atlantic biome (Figure 4a) and Somali Coastal Current System (Figure 4c), one of the world's most productive ecosystems, internal variability uncertainty accounts for more than 54% of total uncertainty in near-term projections of the combined SST, O_2, and NPP stressors, and scenario uncertainty is very small, except for the case of surface pH. Regional analysis will thus often contend with large irreducible uncertainties on this short time frame. There are exceptions, however. Model uncertainty is the dominant uncertainty for O_2 projections averaged over all biomes (Figure 3g) and LMEs (Figure 3k) on multidecadal time scales. Model uncertainty is also prominent in some regions at short time horizons. In the North Atlantic ice biome (Figure 4b) and the Humboldt Current System (Figure 4d), for example, model uncertainty accounts for more than 50% in near-term projections of the combined surface pH, NPP, and O_2 stressors (Figure 4b). Thus, a second aspect of the regional analysis is the large intermodel spread. Resolving intermodel differences could reduce total uncertainty significantly in some specific places such as the North Atlantic ice biome or the Humboldt Current System.

Next we show global spatial snapshots of the relative fractional importance of the three distinct sources of uncertainty to projected annual mean potential stressor states for near-term projections over 2016–2035 (Figure 5) and for longer-term projections over 2076–2095 (Figure 6). For near-term projections, internal

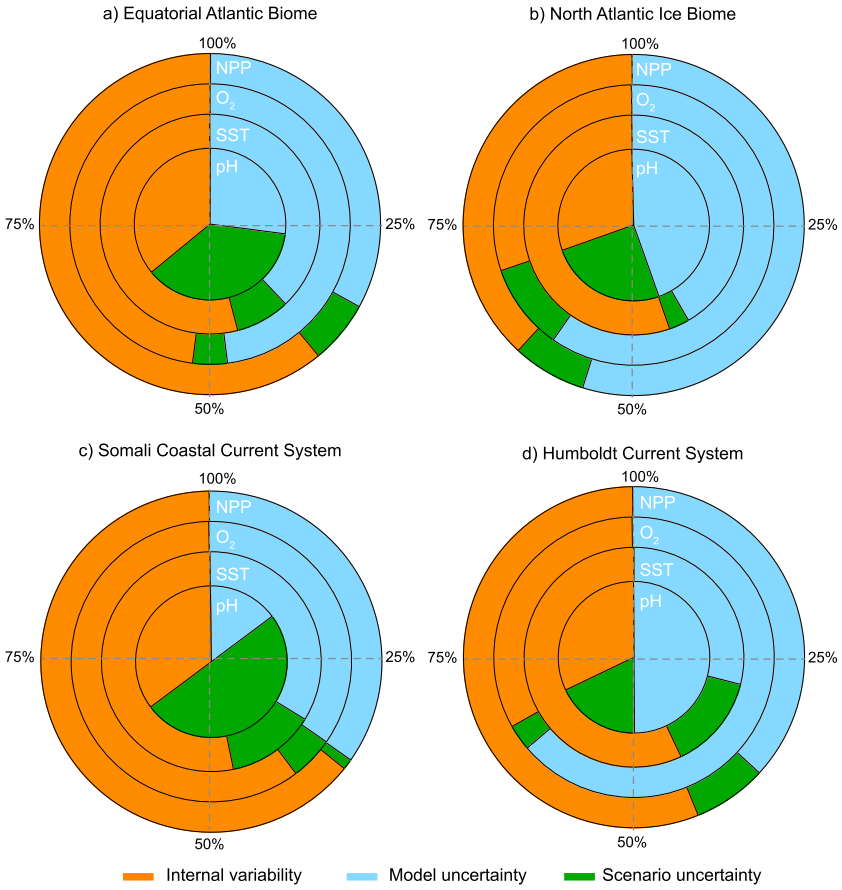

Figure 4. Cocentric pie charts of the fraction of total uncertainty explained by internal variability uncertainty (orange), model uncertainty (blue), and scenario uncertainty (green) in projections of surface pH, SST, O_2 averaged over 100 to 600 m, and NPP integrated over the top 100 m for (a) the equatorial Atlantic biome, (b) the North Atlantic ice biome, (c) the Somali Coastal Current System, and (d) the Humboldt Current System averaged over the near-term interval 2016 to 2035. Within the context of the classification of the biogeographical biomes, the equatorial Atlantic biome and the North Atlantic ice biome are biomes 8 and 12. Within the context of the classification of NOAA's large marine ecosystems (LMEs; http://www.st.nmfs.noaa.gov/ecosystems/lme), the Somali Coastal Current System includes region 31 and the Humboldt Current System includes region 13.

variability uncertainty is dominant in most regions across the middle-to-low latitudes for all four potential ocean ecosystem stressors (Figures 5a, 5d, 5g, and 5j). Model uncertainty is generally high for all potential stressors in regions with open ocean convection such as the Southern Ocean or the North Atlantic and in regions with sea ice coverage such as the Arctic Ocean (Figures 5b, 5e, 5h, and 5k). *Frölicher et al.* [2015] show that the Southern Ocean is the region where models differ the most in representation of heat and carbon uptake and associated changes in biogeochemistry, as the exact processes governing heat and carbon uptake remain poorly understood. For NPP, model uncertainty is large in the southeastern tropical Pacific. There, the models do not even agree on the sign of changes. Scenario uncertainty is small, except for surface pH in the midlatitudes (Figures 5c, 5f, 5i, 5l). The surface waters in the midlatitudes are generally well equilibrated with the atmospheric pCO_2 levels, and therefore, surface pH strongly depends on the future carbon emission pathway.

By the end of the century (Figure 6), scenario uncertainty becomes more prominent in all cases and is dominant for surface pH and low-latitude SST (Figures 6c and 6f). Internal variability uncertainty, however, remains a large source of uncertainty in the annual potential stressor state for NPP (Figure 6j) and O_2 (Figure 6g) in the subtropical gyres. Model uncertainty remains a large source of uncertainty in the Southern Ocean and the North Atlantic for SST (Figure 6e) and in the low latitudes for O_2 (Figure 6h) and NPP (Figure 6k).

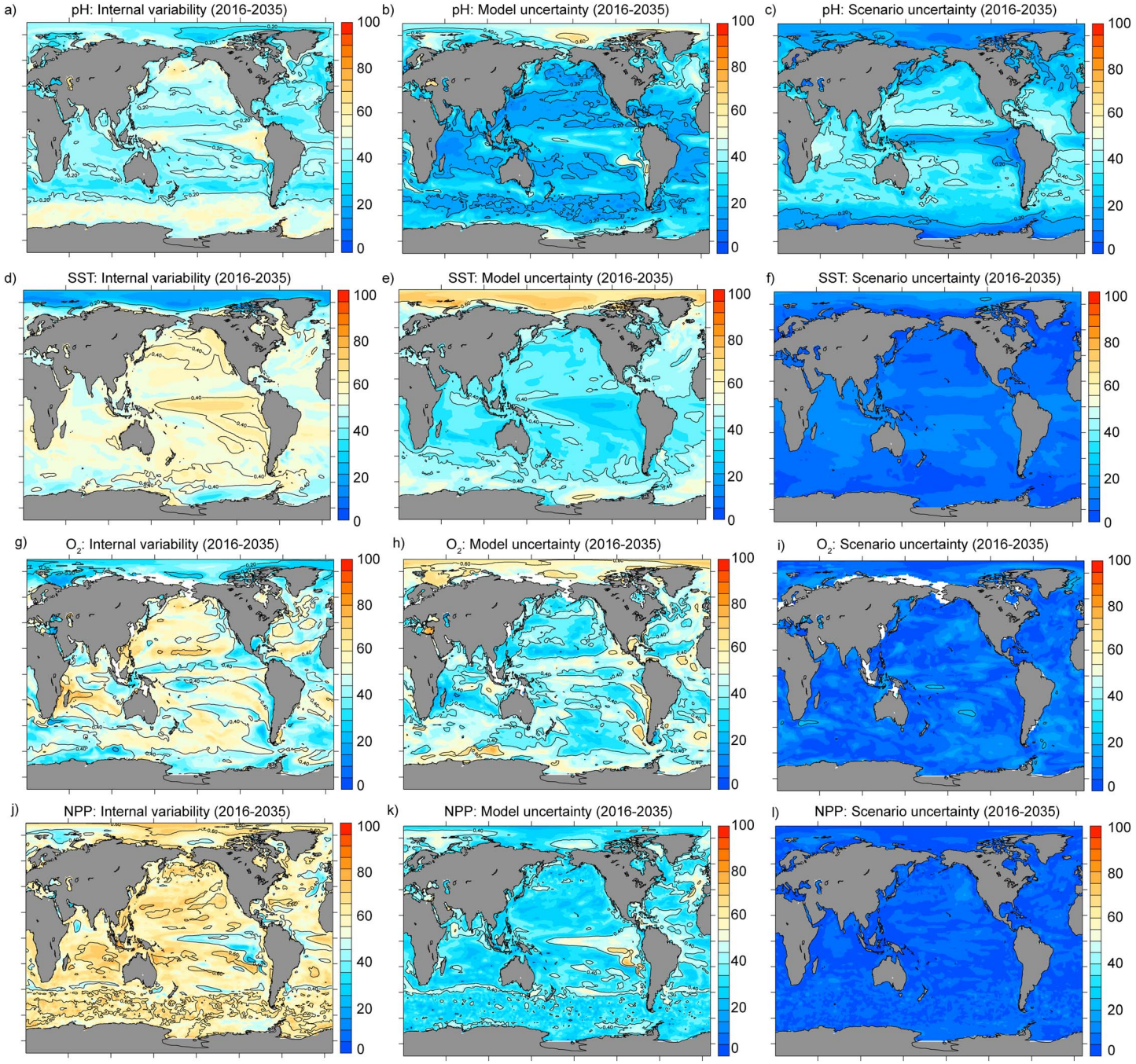

Figure 5. The local fraction of total uncertainty explained by (left column) internal variability uncertainty, (middle column) model uncertainty, and (right column) scenario uncertainty averaged over 2016–2035 period for projections of (a–c) surface pH, (e–f) SST, (g–i) O_2 averaged over 100 to 600 m, and (j–l) NPP integrated over the top 100 m. Units are percentage.

3.4. Time of Emergence in Potential Ocean Ecosystem Stressor Projections

Thus far, we have considered the relationship between the three sources of uncertainty in potential ocean ecosystem stressor projections. As many social-ecological systems are naturally adapted to internal variability, changes in ocean properties that move outside of the internal variability range may most likely trigger impacts that are unprecedented in the recent past [*Pörtner et al.*, 2014; *Cacciapaglia and Woesik*, 2015]. An indicator that is commonly used to quantify such excursions is the signal-to-noise (S/N) ratio [e.g., *Mahlstein et al.*, 2011; *Hawkins and Sutton*, 2012; *Lyu et al.*, 2014], where the signal is a measure of the

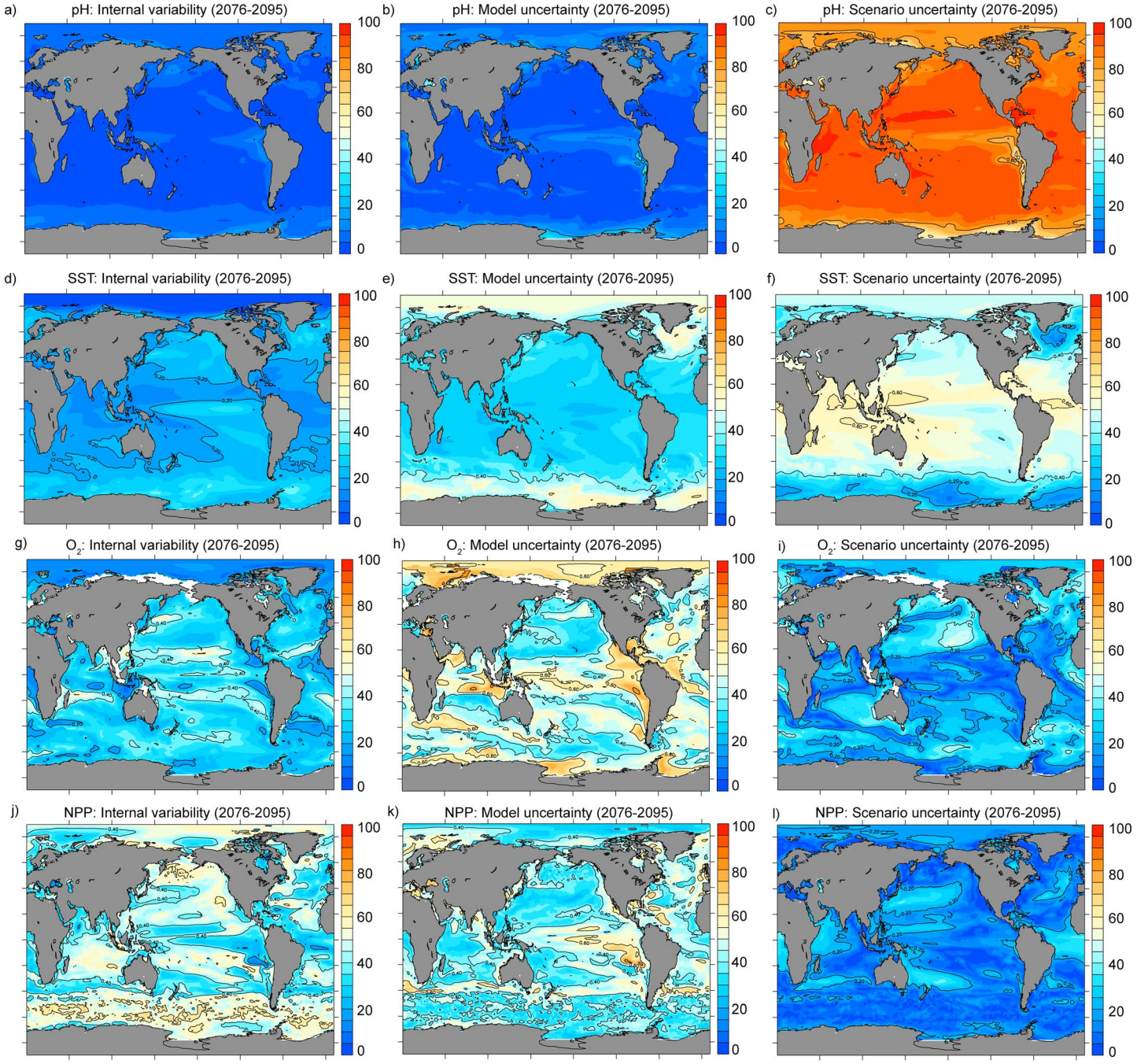

Figure 6. Same as in Figure 5 but averaged over the period of 2076 to 2095.

amplitude of the forced local changes relative to a 1986–2005 reference period and the noise is the sum of local internal and model uncertainties in the projection (see section 2.3).

Figures 7a and 7b show the sensitivity of the S/N ratio of the four potential ocean ecosystem stressors to the RCP8.5 and RCP2.6 greenhouse gas emission scenarios. In the near term (2016–2035), surface pH has a S/N ratio above 1 in all ocean regions regardless of the future carbon emission scenario (gray line in Figures 7a and 7b; 8a). This is in contrast to NPP (blue lines in Figures 7a and 7b; 8d), for which almost no grid cell shows emergence in the near and the long term. Fifty-six percent (38%–71% when using maximum and minimum internal variability estimates from the CMIP5 preindustrial control simulations, respectively) of the ocean area show emergence of the SST signal in the near-term rising to 92% (90%–94%) by the end of the century under

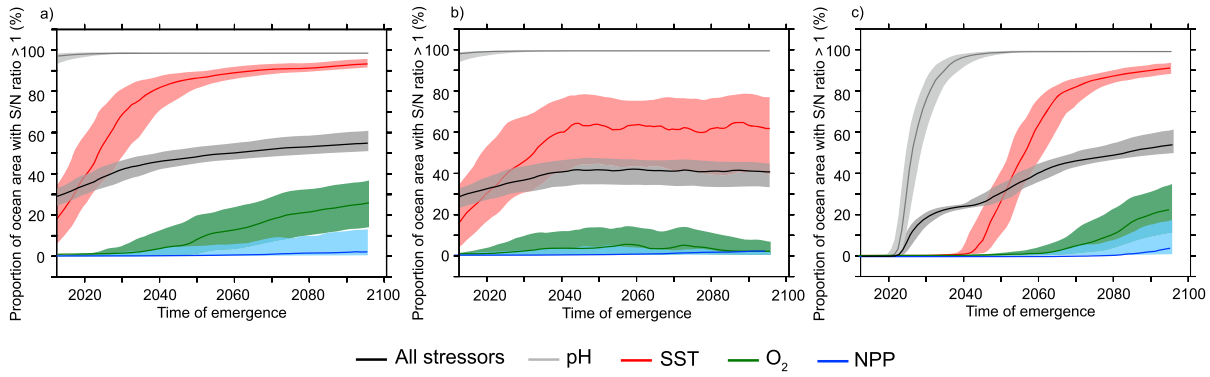

Figure 7. Time series of individual and combined potential ocean ecosystem stressors showing proportion of the ocean area that has a signal-to-noise (S/N) ratio larger than 1 (67% confidence interval) (a) for the business-as-usual scenario RCP8.5 and (b) for the aggressive mitigation scenario RCP2.6 and (c) that experiences a significant difference between the RCP2.6 and the RCP8.5 scenarios. The signal in Figures 7a and 7b is the forced trend (multimodel mean), and the noise is the sum of the model and mean internal variability uncertainties. The black lines in both plots represent an average across the four drivers. The shadings in all plots indicate the uncertainty range when the minimum and maximum internal variability estimates from the CMIP5 preindustrial control simulations are used.

the RCP8.5 scenario (red line in Figure 7a). Under the RCP2.6 scenario, 40% (24%–61%) of the ocean area show emergence of the SST signal in the near term and 62% (39%–76%) by the end of the century (red line in Figure 7b). Early emergence of an SST signal occurs mainly in the low latitudes (Figure 8b) [*Rodgers et al.*, 2015]. However, the Southern Ocean south of 45°S and the North Atlantic experiences no emergence of the signal by the end of the century (Figure 8b). These are both regions, which experience very small warming by

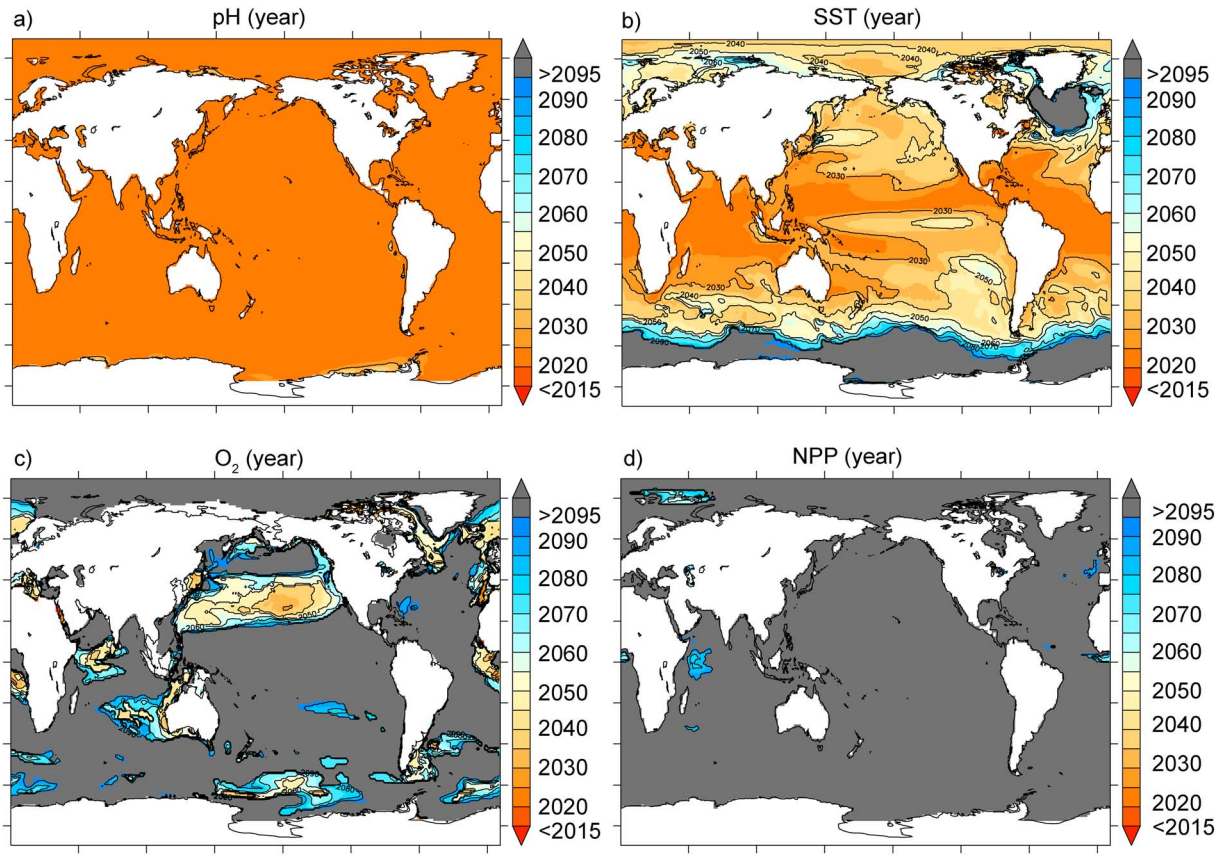

Figure 8. The local time of emergence, calculated using a threshold of 1 standard deviation (67% confidence) for (a) surface pH, (b) SST, (c) O_2 averaged over 100–600 m depth, and NPP integrated over top 100 m. The gray color shows the regions with no emergence by year 2095. The definition of noise includes both mean internal variability uncertainty from all CMIP5 preindustrial control simulations and model uncertainty.

the end of this century (Figures 1e and 1f). In the Southern Ocean, the vigorous wind-driven overturning circulation continues to bring ancient deep cold waters to the surface, which anchors SST to almost preindustrial levels even increasing atmospheric CO_2 levels [*Manabe et al*., 1991; *Morrison et al*., 2015; *Frölicher et al*., 2015]. The cooling feature in the subpolar North Atlantic has been suggested to be a result of a reduced Atlantic meridional overturning circulation under global warming [*Zhang*, 2008; *Winton et al*., 2013]. The oxygen signal emerges very slowly (green lines in Figures 7a and 7b). By the end of this century, 23% (12%–35%; Figure 7a) and 2% (1%–9%; Figure 7b) of the ocean area experience emergence of the O_2 signal under the RCP8.5 and the RCP2.6 scenarios, respectively. As the O_2 concentration is projected to increase after an initial decrease under the RCP2.6 scenario in year 2050 (Figure 1g), the S/N ratio also starts to decrease at around year 2050 under the RCP2.6 scenario. Early emergence is simulated in the midlatitude North Pacific, the Pacific sector of the Southern Ocean, and parts of the northern North Atlantic (Figure 8c). All other regions show no emergence by the end of the century. When combining all four ecosystem drivers, 39% (34%–44%) of the global ocean emerge from the noise averaged over 2016–2035 period and 54% (50%–60%) averaged over 2076–2095 period following the RCP8.5 scenario (black line in Figure 7a). Under the RCP2.6 scenario, 35% (30%–42%) of the global ocean emerge from the noise averaged over 2016–2035 and 41% (35%–47%) averaged over 2076–2095 (black line in Figure 7b).

In general, aggressive mitigation (following the RCP2.6 scenario instead of the RCP8.5 scenario) delays the emergence of the signal substantially (Figure 7a versus Figure 7b). Under the RCP2.6 scenario (Figure 7b), the signal-to-noise ratios are generally smaller than under the RCP8.5 scenario (Figure 7a). In Figure 7c, we emphasize the sensitivity to mitigation and evaluate the time it takes for early aggressive mitigation (i.e., following RCP2.6), having a significant effect on projected changes in the four different ocean ecosystem drivers. Aggressive mitigation would have an effect on 43% (33%–52%) of all ocean areas by 2016–2035 for surface pH (gray line in Figure 7c) and for 30% (18%–45%) of the ocean by 2041–2060 for SST (red line in Figure 7c). Thus, benefits of mitigation are realized rapidly for surface pH and SST, and it is not necessary to wait until the end of the century to see an impact. However, stringent mitigation would not avoid a large proportion of the surface pH and SST changes by the end of the century, as still nearly all (for surface pH) and 62% (39%–76%; for SST) of all ocean surface areas show emergence of the signal under the RCP2.6 scenario by the end of the century (gray and red lines in Figure 7b). Substantial mitigation has only a small effect on O_2 (green line in Figure 7c) and NPP emergence (blue line in Figure 7c): 16% (7%–28%; for O_2) and 2% (0%–12%; NPP) of the ocean area experience significant differences between the paths of aggressive mitigation and business as usual. For the combined setting (black line in Figure 7c), 11% (8%–13%) of the ocean experience changes through mitigation measures in the near term and 51% (48%–58%) by the end of the century. The differences can first be seen in the same regions where also the signal-to-noise ratio is largest (not shown). We note that the emergence of differences between business-as-usual and mitigated states does not necessarily imply a return to preindustrial conditions but may involve novel states during century-scale readjustments [*Frölicher and Joos*, 2010; *John et al*., 2015].

3.5. Sensitivity of Internal Variability Estimates to Calculation Method

The sensitivity of our results to the method applied to calculate internal variability is investigated next. Overall, the differences in simulated internal variability between models from preindustrial control simulations are small for global surface pH (gray bars in Figure 9). However, intermodel differences can be as large as a factor of 3 for global SST (Figure 9b) and O_2 (Figure 9c) and a factor of 4 for global NPP (Figure 9d). We also show that the internal variability estimates from the individual preindustrial control simulations (bars in Figure 9) also differ significantly from the internal variability estimates obtained from detrended transient simulations (points in Figure 9). When estimating internal variability from a large-ensemble simulation with GFDL ESM2M (stars in Figure 9), the variability tends to be higher than estimated with the same model from preindustrial control simulations.

The main result that internal variability is dominant on short time horizons is robust and not very sensitive to the calculation method of internal variability (Figure 10). However, the importance of internal variability for near-term projections differs quantitatively when using different internal variability estimates from different models. This is especially true for SST, O_2, and NPP, for which the importance of internal variability in projections over 2016–2035 can range between 17% and 37% (SST; Figures 10b and 10f), 33% and 51% (O_2; Figures 10c and 10g), and 33% and 63% (NPP; Figures 10d and 10h) when using the minimum and maximum

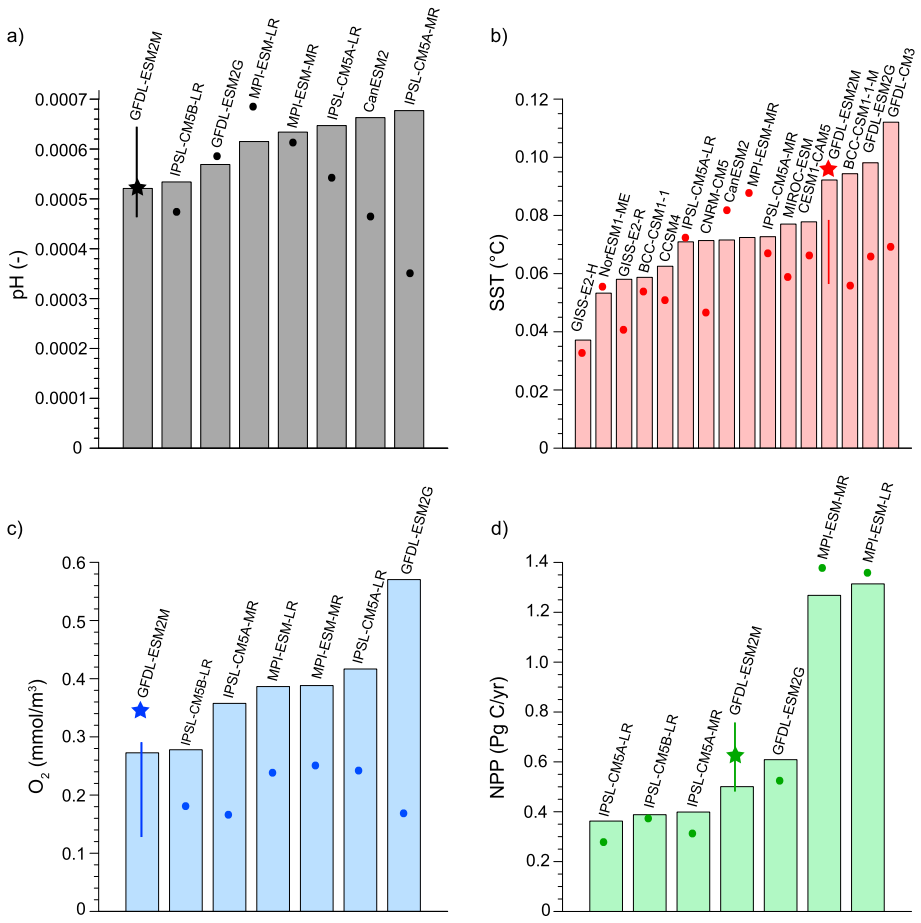

Figure 9. Comparison of internal variability estimates for (a) surface pH, (b) SST, (c) O_2 averaged over 100–600 m depth, and (d) NPP integrated over top 100 m. Internal variability estimates are calculated as 1 standard deviation from annual mean output of century-long preindustrial control simulations (bars), transient simulations over the period of 2006–2100 that have been detrended with a fourth-order polynom (points), and a 30-member ensemble simulation of the GFDL ESM2M (stars). The range of internal variability estimates from the 30 detrended (fourth-order polynom) transient ensemble simulations over the 2006–2100 period of the GFDL ESM2M are shown as uncertainty bars.

internal variability estimates from the CMIP5 preindustrial control simulations. The importance of internal variability for surface pH projections is rather insensitive to the method of calculating internal variability (Figures 10a and 10e). The importance of internal variability for near-term projection only ranges from 10% to 12%.

4. Discussion and Conclusions

We provide a first holistic assessment of the magnitude of changes and the sources of uncertainty in 21st century projections of potential ocean ecosystem stressors at global and regional scales. This has been accomplished by analyzing output from a range of Earth system models that participated in CMIP5. We have demonstrated that internal variability uncertainty is dominant on small spatial scales and short time horizons and that model and in particular scenario uncertainty become dominant in end-of-century projections. Our results also indicate a hierarchy for emergence (defined using signal-to-noise ratio) among the potential ocean ecosystem stressors, with surface pH emerging first, SST second, middepth O_2 third, and NPP fourth. It is worth pointing out that the signal-to-noise ratio for prediction of the potential stressors increases over time, despite model uncertainty also increasing with lead time.

We have chosen herein to focus on the dominant drivers of annual mean potential ocean ecosystem stressor states and thus retained the effects of internal climate variability at subdecadal scales (e.g., ENSO). Other

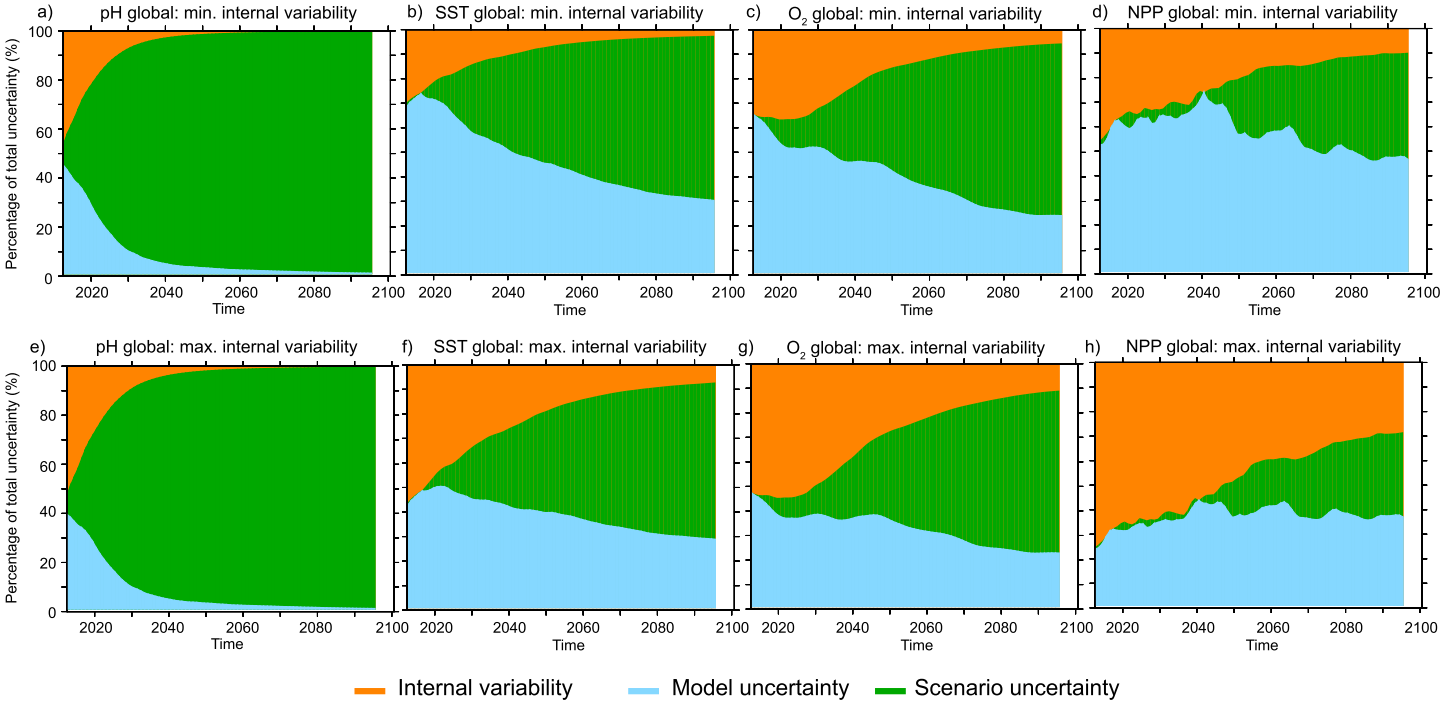

Figure 10. Sensitivity of the sources of uncertainty to internal variability estimates. Fraction of total uncertainty explained by internal variability uncertainty (orange), model uncertainty (blue), and scenario uncertainty (green) in projections of annual mean surface pH, SST, O_2 averaged over 100 to 600 m, and NPP integrated over the top 100 m. The (top row) smallest and (bottom row) largest internal variability estimates from the CMIP5 preindustrial control simulations are used.

analyses, however, have focused on the drivers of uncertainty in decadal mean anomalies and filtered out shorter time scale variations [e.g., *Hawkins and Sutton*, 2009, 2011]. In our analysis, a 10 year low-pass filter applied to global annual mean SST output from the CMIP5 preindustrial control simulations would decrease the contribution of internal variability uncertainty to decadal conditions from 28% (orange area in Figure 11a) to 19% (orange area in Figure 11b) for 2016–2035 projections. However, from the perspective of marine resource management, such treatment greatly underrepresents the degree to which the interannual variations that often shape marine resource patterns are variability dominated. The sensitivity to 10 year low-pass filtering of the scenario and model response uncertainty is less marked. The contribution of internal variability uncertainty of annual conditions is 26% (orange area in Figure 11c) for 2016–2035 global SST projections with CMIP5 when applying a 1 year low-pass filter to scenario and model uncertainties, and the sensitivity does not significantly change the emergent progression of uncertainty with time horizon.

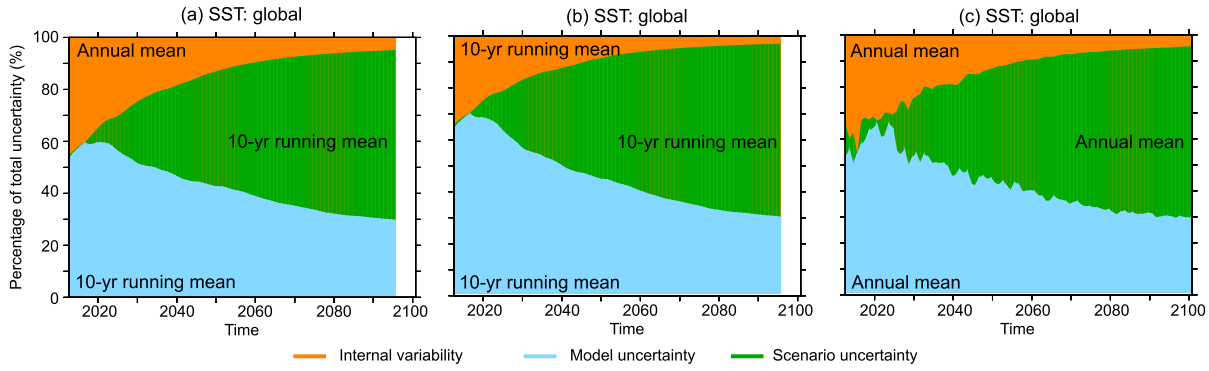

Figure 11. Fraction of total uncertainty explained by internal variability uncertainty (orange), model uncertainty (blue), and scenario uncertainty (green) in projections of global annual mean SST. (a) Same as in Figure 3b, for which CMIP5 annual mean SST projections have been filtered with a 10 year spline and CMIP5 preindustrial control annual mean SST output has not been filtered before calculating the uncertainties. (b) Same as in Figure 11a, but CMIP5 preindustrial control annual mean SST output has been filtered with a 10 year spline before calculating the uncertainties. (c) Same as in Figure 11a, but CMIP5 annual mean SST projections have not been filtered before calculating the uncertainties.

Importantly, the relatively elevated contribution of internal variability uncertainty over near-term time horizons and regional scales is expected to be robust and not an artifact of the method chosen here for analysis. Nevertheless, the importance of internal variability uncertainty is modestly sensitive to the approach used for characterizing the variability itself and the associated time scale of variability. We have shown that the internal variability estimates on a global scale from the different methods can differ by more than a factor of 3 for SST and O_2 and by a factor of 4 for NPP (Figure 9). Ideally, one would like to have large-ensemble simulations from a range of different climate models to truly sample the variability [*Frölicher et al*., 2009; *Deser et al*., 2012; *Christian*, 2014; *Deser et al*., 2014; *Rodgers et al*., 2015; *McKinley et al*., 2016]. The large ensemble captures the evolution of modes of variability as the ocean responds to greenhouse gas forcing and captures all time scales of variability. However, these large-ensemble simulations are computationally expensive and only a limited set of ensembles are currently available [e.g., *Frölicher et al*., 2009; *Kay et al*., 2015; *Rodgers et al*., 2015]. Thus, the calculation of internal variability using preindustrial control simulations currently stands as the best way for estimating internal variability within a holistic evaluation of uncertainty until an increasing numbers of large ESM ensembles become available.

It is important to consider the implications of our results for prioritizing resource allocation with the larger goal of reducing uncertainties in future projections of potential ocean ecosystem stressors. Our consideration of biogeographical biomes and large marine ecosystems served to emphasize the continued importance of internal variability uncertainty for near-term regional and local projections as has been exemplified for the equatorial Atlantic biome (Figure 4a) and the Somali Coastal Current System (Figure 4c). In this way, our analysis is fully consistent with earlier studies that suggest that internal variability uncertainty is central for near-term projections on a regional-to-local scale [*Hawkins and Sutton*, 2009, 2011]. This underscores the importance of large initial condition ensemble runs with multiple ESMs [*Kay et al*., 2015; *Rodgers et al*., 2015], in parallel with efforts to better understand the limits to near-term predictability and improvement of model skill in representing interannual-to-decadal variability. Recent studies reveal that improved initial conditions may lead to improved predictive skill in SST and NPP forecasts on time scales of a few years [*Séférian et al*., 2014; *Stock et al*., 2015; *Meehl et al*., 2014]. For the physical state of the system, however, the dominant barrier to predictability may not be initialization skill but rather inherent nonlinearities in the climate system [*Wittenberg et al*., 2014]. Addressing these questions further within the context of potential ocean ecosystem stressors should be part of an integrated future assessment of uncertainty.

On a global scale, uncertainty in century-scale projections due to disparate future greenhouse gas emission scenarios (here referred to scenario uncertainty) is larger than internal and model uncertainties. However, the model uncertainty contribution is larger than the internal variability uncertainty contribution toward the end of the 21st century for all four drivers, in particular, for O_2 and NPP predictions. Even in near-term projections, model uncertainty may be dominant for thermocline O_2 projections and in specific regions, such as the North Atlantic ice biome (Figure 4b) and the Humboldt Current System (Figure 4d). This underscores the critical importance of improved process representation and improved parameterizations in modeling tools in reducing uncertainty. New observations, advances in theory, improved modeling, and new methods for bringing together models and observations can be expected to deliver significant progress in this area.

Our analysis also has important consequences for assessing impacts and vulnerability of marine biodiversity and ecosystem services. Recent studies have suggested that ocean acidification and warming are already impacting marine biodiversity [*Pörtner et al*., 2014] and fisheries [*Cheung et al*., 2013], particularly in low-latitude regions and in particular for sensitive ecosystems such as coral reefs [*Gattuso et al*., 2014]. It is expected that future changes in the physical and biogeochemical conditions of the ocean will increase the risk of severe, pervasive, and irreversible impacts on composition, structure, and functioning of ocean ecosystems, subsequently altering fishery catches and cultural services [*Intergovernmental Panel on Climate Change*, 2014; *Gattuso et al*., 2015]. Here risk implies a significant probability that something will happen but does not imply that it will happen for certain. Thus, the simulated early emergence of surface pH and low-latitude SST signals from the noise (Figures 7a, 7b, and 8) suggest high risk of impacts on ocean ecosystems sensitive to pH and temperature changes in these regions, consistent with previous results obtained with the 30-member ensemble with GFDL's ESM2M [*Rodgers et al*., 2015].

We also show that changes in surface pH and SST can be reduced substantially and rapidly with aggressive mitigation of carbon emissions (Figure 7c), highlighting the potential benefits to marine ecosystem services

through risk reduction. In contrast, the low signal-to-noise ratios in Southern Ocean warming, oxygen concentrations in low-O_2 waters, and NPP predictions over the next few decades, and in general in large marine ecosystems, suggest that adaptation decisions needs to be made in the context of high uncertainty. This is of particular concern as recent studies suggest that changes in O_2 level and NPP may also impact species biogeography and potential fishery catches [*Pörtner et al*., 2014; *Jones and Cheung*, 2015], adding to the uncertainties of projecting future living marine resources [*Cheung et al*., 2016]. Identifying fishery management and conservation policies that are cognizant and respectful of such elevated uncertainty is thus of great importance to facilitating adaptation to climate change impacts in the oceans.

Throughout this study, we have chosen to use the qualifier "potential" ocean ecosystem stressors to include changes that may in some instances and regions be beneficial for marine ecosystems. For example, expanding O_2 minimum zones may restrict the habitat of O_2-dependent organisms but may also benefit anaerobic microbes [*Pörtner et al*., 2014]. Increasing NPP in high latitudes may also be beneficial. A better understanding of interaction mechanisms and capacity for adaption is needed to fully understand their impact on marine resources and is expected to be subject of exploratory research for some time to come [*Gunderson et al*., 2016].

Improved regional climate simulations are a focal point of current research in the application of climate modeling. Such work is intended to facilitate the formulation of marine resource management strategies. Although the spatial resolution of global climate models will steadily increase in the future, improving the process representation of critical scales regionally, downscaling will continue to play a critical role in improving regional assessment of marine ecosystems and fishery impacts under climate change. Taking regional applications of the models considered here as an example, the critical spatial scales for skillful representation of the system state is often significantly smaller than what the models explicitly resolve. For this reason, regional downscaling provides an important tool for evaluating regional impacts [e.g., *Gruber et al*., 2012]. Nevertheless, progress with downscaling approaches faces significant challenges [*Xie et al*., 2015]. To date, downscaling exercises (for example, with eastern boundary upwelling systems or fishery models) tend to be conducted with single climate projections with one Earth system model [e.g., *Gruber et al*., 2012; *Cheung et al*., 2010]. Our analysis reveals that internal variability uncertainty and model uncertainty can be substantial, with such uncertainties in projections being expected to propagate to fishery impact assessments, particularly for NPP. It is important to emphasize that although the representation of variability at regional scales will undoubtly be impacted by missing scales and processes for some time to come, our results of the predominance of variability uncertainty with regional projections is unlikely to be affected. For this reasons, our study suggests prioritizing expanded and improved multimodel and large initial condition ensemble projections with Earth system models to the end of evaluating regional marine resource impacts [e.g., *Jones et al*., 2013; *Cheung et al*., 2012] and to incorporate the expanded ensemble approach into downscaling applications.

Acknowledgments
We thank N. Gruber and J.L. Sarmiento for their constructive discussions and J.P. Dunne for their comments on the manuscript. T.L. Frölicher acknowledges financial support from the SNSF (Ambizione grant PZ00P2_142573). The support of K.B. Rodgers comes through awards NA17RJ2612 and NA08OAR4320752, including support through the NOAA Office of Climate Observations, NOAA award NA11OAR4310066, and NASA award NNX14AL85G. W.W.L. Cheung and T.L. Frölicher acknowledge support from the Nippon Foundation-UBC Nereus Program, and W.W.L. Cheung acknowledges support from Natural Sciences and Engineering Research Council of Canada. We acknowledge the World Climate Research Programme's Working Group on Coupled Modelling, which is responsible for CMIP, and we thank the climate modeling groups (listed in Table S1 of this paper) for producing and making available their model output. We thank S. Schmidtko and S. Lauvset for providing observation-based O_2 and pH data products.

References

Behrenfeld, M. J., R. T. O'Malley, D. A. Siegel, C. R. McClain, J. L. Sarmiento, G. C. Feldman, A. J. Milligan, P. G. Falkowski, R. M. Letelier, and E. S. Boss (2006), Climate-driven trends in contemporary ocean productivity, *Nature*, *444*, 752–755.

Booth, B. B. B., D. Bernie, D. McNeall, E. Hawkins, J. Caesar, C. Boulton, P. Friedlingstein, and D. M. H. Sexton (2013), Scenario and modeling uncertainty in global mean temperature change derived from emission-driven global climate models, *Earth Syst. Dyn.*, *4*, 95–108.

Bopp, L., P. Monfray, O. Aumont, J.-L. Dufresne, H. Le Treut, G. Madec, L. Terray, and J. C. Orr (2001), Potential impact of climate change on marine export production, *Global Biogeochem. Cycles*, *15*, 81–99, doi:10.1029/1999GB001256.

Bopp, L., et al. (2013), Multiple stressors of ocean ecosystems in the 21st century: Projections with CMIP5 models, *Biogeosciences*, *10*, 6225–6245.

Bordbar, M. H., T. Martin, M. Latif, and W. Park (2015), Effects of long-term variability on projections of twenty-first century dynamic sea level, *Nat. Clim. Change*, *5*, 343–347.

Cacciapaglia, C., and R. Woesik (2015), Reef-coral refugia in a rapidly changing ocean, *Global Change Biol.*, *21*, 2272–2282.

Cane, M. A., and S. E. Zebiak (1985), A theory for El Niño and the Southern Oscillation, *Science*, *228*, 1085–1087.

Capotondi, A., M. A. Alexander, N. A. Bond, E. N. Curchitser, and J. D. Scott (2012), Enhanced upper ocean stratification with climate change in the CMIP3 models, *J. Geophys. Res.*, *117*, C04031, doi:10.1029/2011JC007409.

Cheung, W. W. L., V. W. Y. Lam, J. L. Sarmiento, K. Kearney, R. Watson, D. Zeller, and D. Pauly (2010), Large-scale redistribution of maximum fisheries catch potential in the global ocean under climate change, *Global Change Biol.*, *16*, 24–35.

Cheung, W. W. L., J. Meeuwig, M. Feng, E. Harvey, V. W. H. Lam, T. Langlois, D. Slawinski, C. Sun, and D. Pauly (2012), Climate-change induced tropicalisation of marine communities in Western Australia, *Mar. Freshwater Res.*, *3*, 415–427.

Cheung, W. W. L., D. Pauly, and J. L. Sarmiento (2013), How to make progress in projecting climate change impacts, *J. Mar. Sci.: J. Cons.*, *70*(6), 1069–1074.

Cheung, W. W. L., et al (2016), Building confidence in projections of the responses of living marine resources to climate change, *J. Mar. Sci.*, doi:10.1093/icesjms/fsv250.
Christian, J. R. (2014), Timing of the departure of ocean biogeochemical cycles from the preindustrial state, *PLoS One*, *9*, e109820.
Cocco, V., et al. (2013), Oxygen and indicators of stress for marine life in multi-model global warming projections, *Biogeosciences*, *10*, 1849–1868.
Collins, M., et al. (2013), Long-term climate change: Projections, commitments and irreversibility, in *Climate Change 2013: The Physical Science Basis. Contribution of Working Group I to the Fifth Assessment Report of the Intergovernmental Panel on Climate Change*, edited by T. F. Stocker et al., Cambridge Univ. Press, Cambridge, U. K., and New York.
Crain, C. M., K. Kroeker, and B. S. Halpern (2008), Interactive and cumulative effects of multiple human stressors in marine systems, *Ecol. Lett.*, *11*, 1304–1315.
Deser, C., R. Knutti, S. Solomon, and A. S. Phililips (2012), Communication of the role of natural variability in future North American climate, *Nat. Clim. Change*, *2*, 775–779.
Deser, C., A. S. Phillips, M. A. Alexander, and B. V. Smoliak (2014), Projecting North American climate over the next 50 years: Uncertainty due to internal variability, *J. Clim.*, *27*, 2271–2296.
Doney, S. C., V. J. Fabry, R. A. Feely, and J. A. Kleypas (2009), Ocean acidification: The other CO_2 problem, *Annu. Rev. Mar. Sci.*, *1*, 169–192.
Doney, S. C., et al. (2012), Climate change impacts on marine ecosystems, *Annu. Rev. Mar. Sci.*, *4*, 11–37.
Dunne, J. P., et al. (2012), GFDL's ESM2 global coupled climate-carbon Earth system models. Part I: Physical formulation and baseline simulation characteristics, *J. Clim.*, *25*, 6646–6665.
Dunne, J. P., et al. (2013), GFDL's ESM2 global coupled climate-carbon Earth system models. Part II: Carbon system formulation and baseline simulation characteristics, *J. Clim.*, *26*, 2247–2267.
Fay, A. R., and G. A. McKinley (2014), Global open-ocean biomes: Mean and temporal variability, *Earth Syst. Sci. Data*, *6*, 273–284.
Frölicher, T. L., and F. Joos (2010), Reversible and irreversible impacts of greenhouse gas emissions in multi-century projections with the NCAR global coupled carbon cycle-climate model, *Clim. Dyn.*, *35*, 1439–1459.
Frölicher, T. L., F. Joos, G.-K. Plattner, M. Steinacher, and S. C. Doney (2009), Natural variability and anthropogenic trends in oceanic oxygen in a coupled carbon cycle-climate model ensemble, *Global Biogeochem. Cycles*, *23*, GB1003, doi:10.1029/2008GB003316.
Frölicher, T. L., J. L. Sarmiento, D. J. Paynter, J. P. Dunne, J. P. Krasting, and M. Winton (2015), Dominance of the Southern Ocean in anthropogenic carbon and heat uptake in CMIP5 models, *J. Clim.*, *28*, 862–886.
Gattuso, J.-P., O. Hoegh-Guldberg, and H.-O. Pörtner (2014), Coral reefs, in *Climate Change 2014: Impacts, Adaptation and Vulnerability. Contribution of Working Group II to the Fifth Assessment Report of the Intergovernmental Panel on Climate Change*, edited by C. B. Field et al., pp. 97–100, Cambridge Univ. Press, Cambridge, U. K.
Gattuso, J.-P., et al. (2015), Contrasting futures for ocean and society from different anthropogenic CO_2 emissions scenarios, *Science*, *349*(6243), aac4722.
Gruber, N. (2011), Warming up, turning sour, losing breath: Ocean biogeochemistry under global change, *Philos. Trans. R. Soc. A*, *369*, 1980–1996.
Gruber, N., C. Hauri, Z. Lachkar, D. Loher, T. L. Frölicher, and G.-K. Plattner (2012), Rapid progression of ocean acidification in the California Current System, *Science*, *337*, 220–223.
Gunderson, A. R., E. J. Armstrong, and J. H. Stillman (2016), Multiple stressors in a changing world: The need for an improved perspective on physiological responses to the dynamic marine environment, *Annu. Rev. Mar. Sci.*, *8*, 12.1–12.22.
Hall, J., R. J. Diaz, N. Gruber, and D. Wilhelmson (2013), The impacts of multiple stressors. A complex web of challenges, in *Managing Ocean Environments in a Changing Climate*, edited by K. J. Noone, U. S. Sumalia, and R. J. Diaz, pp. 193–222, Elsevier, Burlington, Mass.
Halpern, B. S., et al. (2008), A global map of human impact on marine ecosystems, *Science*, *319*, 948–952.
Hawkins, E., and R. Sutton (2009), The potential to narrow uncertainty in regional climate predictions, *Bull. Am. Meteorol. Soc.*, *90*, 1095–1107.
Hawkins, E., and R. Sutton (2011), The potential to narrow uncertainty in projections of regional precipitation change, *Clim. Dyn.*, *37*, 407–418.
Hawkins, E., and R. Sutton (2012), Time of emergence of climate signals, *Geophys. Res. Lett.*, *39*, L01702, doi:10.1029/2011GL050087.
Hoegh-Guldberg, O., and J. F. Bruno (2010), The impact of climate change on the world's marine ecosystems, *Science*, *328*, 1523–1528.
Huttingford, C., P. D. Jones, V. N. Livina, T. M. Lenton, and P. M. Cox (2013), No increase in global temperature variability despite changing regional patterns, *Nature*, *500*, 327–330.
IPCC (2014), Summary for policymakers, in *Climate Change 2014: Impacts, Adaption, and Vulnerability. Part A: Global and Sectoral Aspects. Contribution of Working Group II to the Fifth Assessment Report of the Intergovernmental Panel on Climate Change*, edited by C. B. Field et al., pp. 1–32, Cambridge Univ. Press, Cambridge, U. K.
John, J. G., C. A. Stocker, and J. P. Dunne (2015), A more productive, but different, ocean after mitigation, *Geophys. Res. Lett.*, *42*, 9836–9845, doi:10.1002/2015GL066160.
Jones, M. C., and W. W. L. Cheung (2015), Multi-model ensemble projections of climate change effects on global marine biodiversity, *ICES J. Mar. Sci.*, *72*, 741–752.
Jones, M. C., S. R. Dye, J. A. Fernandes, T. L. Frölicher, J. K. Pinnegar, R. Warren, and W. W. L. Cheung (2013), Predicting the impact of climate change on threatened species in UK waters, *PLoS One*, *8*, e54216.
Kay, J. E., et al. (2015), The Community Earth System Model (CESM) large ensemble project: A community resource for studying climate change in the presence of internal climate variability, *Bull. Am. Meteorol. Soc.*, *96*, 1333–1349.
Keeling, R. F., A. Körtzinger, and N. Gruber (2010), Ocean deoxygenation in a warming world, *Annu. Rev. Mar. Sci.*, *2*, 199–229.
Keller, K. M., F. Joos, and C. C. Raible (2014), Time of emergence of trends in ocean biogeochemistry, *Biogeosciences*, *11*, 3647–3659.
Knutti, R., D. Masson, and A. Gettelman (2013), Climate model genealogy: Generation CMIP5 and how we got there, *Geophys. Res. Lett.*, *40*, 1194–1199, doi:10.1002/grl.50256.
Kroeker, K. J., R. L. Kordas, R. Crim, I. E. Hendriks, L. Ramajo, G. S. Singh, C. M. Duarte, and J. P. Gattuso (2013), Impacts of ocean acidification on marine organisms: Quantifying sensitivities and interaction with warming, *Global Change Biol.*, *19*(6), 1884–1896.
Laufkötter, C., et al. (2015), Drivers and uncertainties of future global marine primary production in marine ecosystem models, *Biogeosci. Discuss.*, *12*, 3731–3824.
Lauvset, K., N. Gruber, P. Landschützer, A. Olson, and J. Tjiputra (2015), Trends and drivers in global surface ocean pH over the past 3 decades, *Biogeosciences*, *12*, 1285–1298.
Link, J. S., T. F. Ihde, C. J. Harvey, S. K. Gaichas, J. C. Field, J. K. T. Brodziak, H. M. Townsend, and R. M. Peterman (2012), Dealing with uncertainty in ecosystem models: The paradox of use for living marine resource management, *Prog. Oceanogr.*, *102*, 102–114.
Little, C., R. M. Horton, R. E. Kopp, M. Oppenheimer, and S. Yip (2015), Uncertainty in twenty-first century CMIP5 sea level projections, *J. Clim.*, *28*, 838–852.

Lorenz, E. N. (1963), Deterministic nonperiodic flow, *J. Atmos. Sci.*, *20*, 130–141.
Lovenduski, N., G. A. McKinley, A. R. Fay, K. Lindsay, and M. C. Long (2016), Partitioning uncertainty in ocean carbon uptake projections, *Global Biogeochem. Cycles*, doi:10.1002/2016GB005426, in press.
Lyu, K., X. Zhang, J. A. Church, A. B. A. Slangen, and J. Hu (2014), Time of emergence for regional sea-level change, *Nat. Clim. Change*, *4*, 1006–1010.
Lyu, K., X. Zhang, J. A. Church, and J. Hu (2015), Quantifying internally-generated and externally-forced climate signal at regional scales in CMIP5 models, *Geophys. Res. Lett.*, *42*, 9394–9403, doi:10.1002/2015GL065508.
Mahlstein, I., R. Knutti, S. Solomon, and R. Portmann (2011), Early onset of significant local warming in low latitude, *Environ. Res. Lett.*, *6*, 034009.
Manabe, S., R. J. Stouffer, M. J. Spelman, and K. Bryan (1991), Transient response of a coupled ocean-atmosphere model to gradual changes of atmospheric CO_2. Part I. Annual mean response, *J. Clim.*, *4*, 785–818.
McKinley, G. A., et al. (2016), Timescales for detection of trends in the ocean carbon sink, *Nature*, *530*, 469–472.
McNeil, B. I., and T. P. Sasse (2016), Future ocean hypercapnia driven by anthropogenic amplification of the natural CO_2 cycle, *Nature*, *529*, 383–386.
Meehl, G. A., et al. (2014), Decadal climate prediction: An update from the trenches, *Bull. Am. Meteorol. Soc.*, *95*, 243–267.
Morrison, A. K., T. L. Frölicher, and J. L. Sarmiento (2015), Upwelling in the Southern Ocean, *Phys. Today*, *68*, 27–32.
Murphy, J. M., D. M. H. Sexton, D. N. Barnett, G. S. Jones, M. J. Webb, M. Collins, and D. A. Stainforth (2004), Quantification of modeling uncertainties in a large ensemble of climate change simulations, *Nature*, *430*, 768–772.
Pauly, D., et al. (2008), Fisheries in large marine ecosystems: descriptions and diagnoses, in *The UNEP Large Marine Ecosystems Report: A Perspective on Changing Conditions in LMEs of the Worlds Regional Seas*, *UNEP Reg. Seas Rep. and Stud.*, vol. 182, edited by K. Sherman and G. Hempel, pp. 23–40.
Pörtner, H. O., et al. (2014), Ocean system, in *Climate Change 2014: Impacts, Adaptation, and Vulnerability. Part A: Global and Sectoral Aspects. Contribution of Working Group II to the Fifth Assessment Report of the Intergovernmental Panel on Climate Change*, edited by C. B. Field et al., pp. 411–484, Cambridge Univ. Press, Cambridge, U. K.
Resplandy, L., R. Séférian, and L. Bopp (2015), Natural variability of CO_2 and O_2 fluxes: What can we learn from centuries-long climate model simulations?, *J. Geophys. Res. Oceans*, *120*, 384–404, doi:10.1002/2014JC010463.
Rhein, M., et al. (2013), Observations: Ocean, in *Climate Change 2013: The Physical Science Basis. Contribution of Working Group I to the Fifth Assessment Report of the Intergovernmental Panel on Climate Change*, edited by T. F. Stocker et al., Cambridge Univ. Press, Cambridge, U. K., and New York.
Rodgers, K. B., et al. (2009), Using altimetry to help explain patchy changes in hydrographic carbon measurements, *J. Geophys. Res.*, *114*, C09013, doi:10.1029/2008JC005183.
Rodgers, K. B., J. Lin, and T. L. Frölicher (2015), Emergence of multiple ocean ecosystem drivers in a large ensemble suite with an Earth system model, *Biogeosciences*, *12*, 3301–3320.
Sabine, C. L., et al. (2004), The ocean sink for anthropogenic CO_2, *Science*, *305*, 367–371.
Sarmiento, J. L., T. M. C. Hughes, R. J. Stouffer, and S. Manabe (1998), Simulated response of the ocean carbon cycle to anthropogenic climate warming, *Nature*, *393*, 245–249.
Screen, J. A. (2014), Arctic amplification decreases temperature variance in northern mid-to-high latitudes, *Nat. Clim. Change*, *4*, 577–582.
Séférian, R., L. Bopp, M. Gehlen, D. Swingedouw, J. Mignot, E. Guilyardi, and J. Servonnat (2014), Multi-year predictability of tropical marine productivity, *Proc. Natl. Acad. Sci. U.S.A.*, *111*, 11,646–11,651.
Sherman, K., and L. M. Alexander (1986), *Variability and Management of Large Marine Ecosystems*, *AAAS Sel. Symp. 99*, 319 pp., Westview, Boulder, Colo.
Smith, T. M., R. W. Reynolds, T. C. Peterson, and J. Lawrimore (2008), Improvements to NOAA's historical merged land-ocean surface temperature analysis (1880-2006), *J. Clim.*, *21*, 2283–2296.
Steinacher, M., et al. (2010), Projected 21st century decrease in marine productivity: A multi-model analysis, *Biogeosciences*, *7*, 979–1005.
Stock, C. A., et al. (2011), On the use of IPCC-class models to assess the impact of climate on living marine resources, *Prog. Oceanogr.*, *88*, 1–27.
Stock, C. A., et al. (2015), Seasonal sea surface temperature anomaly prediction for coastal ecosystems, *Prog. Oceanogr.*, *137*, 219–236.
Stramma, L., A. Oschlies, and S. Schmidtko (2012), Mismatch between observed and modeled trends in dissolved upper-ocean oxygen over the last 50 yr, *Biogeosciences*, *9*, 4045–4057.
Taylor, K. E., R. J. Stouffer, and G. A. Meehl (2012), An overview of CMIP5 and the experiment design, *Bull. Am. Meteorol. Soc.*, *93*(4), 485–498.
Van Vuuren, D. P., et al. (2011), The representative concentration pathways: An overview, *Clim. Change*, *109*, 5–31.
Winton, M., S. M. Griffies, B. Samuels, J. L. Sarmiento, and T. L. Frölicher (2013), Connecting changing ocean circulation with changing climate, *J. Clim.*, *26*, 2268–2278.
Wittenberg, A. T., A. Rosati, T. L. Delworth, G. A. Vecchi, and F. Zeng (2014), ENSO modulations: Is it decadally predictable?, *J. Clim.*, *27*, 2667–2681.
Xie, S.-P., et al. (2015), Towards predictive understanding of regional climate change, *Nat. Clim. Change*, *5*, 921–930.
Yip, S., C. A. T. Ferro, and D. B. Stephenson (2011), A simple coherent framework for partitioning uncertainty in climate predictions, *J. Clim.*, *24*, 4634–4643.
Zhang, R. (2008), Coherent surface-subsurface fingerprint of the Atlantic meridional overturning circulation, *Geophys. Res. Lett.*, *35*, L20705, doi:10.1029/2008GL035463.